IEEE Access
Multidisciplinary | Rapid Review | Open Access Journal

Received 1 February 2024, accepted 12 February 2024, date of publication 1 March 2024, date of current version 7 March 2024.

Digital Object Identifier 10.1109/ACCESS.2024.3372861

RESEARCH ARTICLE

Coaxial Magnetic Gear-Based Tool-Changing System

HANGYEOL SONG, JUNGWOO HUR, AND SEOKHWAN JEONG, (Member, IEEE)
Department of Mechanical Engineering, Sogang University, Seoul 04107, South Korea

Corresponding author: Seokhwan Jeong (seokhwan@sogang.ac.kr)

This work was supported in part by the National Research Foundation of Korea (NRF) grant funded by the Korean Government (MSIT) under Grant 2021R1F1A1046838 and Grant RS-2023-00218379; in part by the Technology Innovation Program funded by the Ministry of Trade, Industry & Energy (MOTIE, South Korea) under Grant 20018274; and in part by Korea Institute for Advancement of Technology (KIAT) grant funded by the Korean Government (MOTIE) (HRD Program for Industrial Innovation) under Grant P0020535.

ABSTRACT This paper presents a novel tool-changing mechanism that leverages a coaxial magnetic gear (CMG) with non-contact torque control capability. The non-contact power transmission feature of the magnetic gear provides not only sensorless torque control for rotational motion but also easy attachment/detachment without requiring additional actuation. Moreover, the isolation of the powertrain makes it resilient to external impacts. To facilitate tool replacement, we have introduced a docking station equipped with gas springs and an additional degree of freedom. This enables robust tool plate interchangeability without concerns about disturbances during the attachment process. We also established an integrated control structure by building upon our prior research, and the prototype of the proposed mechanism was validated through experimentation using a 6-degree of freedom (DoF) robotic manipulator.

INDEX TERMS Mechanism design, factory automation, actuation and joint mechanisms.

I. INTRODUCTION

As the robot industry continues to advance significantly, the adoption of manipulators for manufacturing automation is becoming increasingly popular. This is primarily driven by their benefits in terms of repeatability, reliability, and the ease of achieving mass personalization [1]. Furthermore, manipulators are not solely confined to factory automation; they find utility across a diverse range of environments when integrated with mobile robots. Even quadruped robots [2], [3] equipped with a 6-DoF manipulator and gripper are capable of performing mobile manipulation tasks, such as opening doors, turning valves, and manipulating various objects.

However, the manufacturing or manipulation process often involves multiple intricate tasks that cannot be adequately handled by a robot equipped with a single end-effector, leading to additional human interventions or universal end-effector designs. Several research groups and companies have been working to tackle this issue through unique approaches [4], [5], [6], [7], such as the dual tool-flange mechanism [4], adaptive grippers that use granular jamming [6], dielectric elastomer [5], and fin-lay mechanisms [7]; However, the universal end-effector designs could limit specific task-oriented manipulations such as bolting, assembling, and milling.

Other approaches have been addressing this challenge by implementing automated tool-changing mechanisms, which involve switching the mounted tools to adapt to different tasks. The automatic tool changers enable a robotic manipulator to seamlessly employ various tools or end-effectors, eliminating the necessity for human intervention during the tool transition procedure. Table 1 shows a comparison of commercially available tool changers' coupling and actuation methods. The automatic tool changers (SWS 005, Schunk [8] and QC, ATI [9]) employ a pneumatic source to actuate the coupling mechanism consisting of a taper and multiple balls. The electric quick changer (EQC5, Gimatic [10]) employs the coupling mechanism consisting of multiple balls driven by an electric motor to lock and unlock the end-effector. Nordbo Robotics [11] employs an electro-permanent magnet (EPM) mechanism that utilizes high voltage to magnetize and demagnetize permanent magnets, enabling the assembling and disassembling of the tools. TripleA robotics [12] employs a passive mechanism to change the tools using specially designed docking stations. Still, the most automated tool chaining mechanisms necessitate extra actuation for locking

The associate editor coordinating the review of this manuscript and approving it for publication was Hongli Dong.

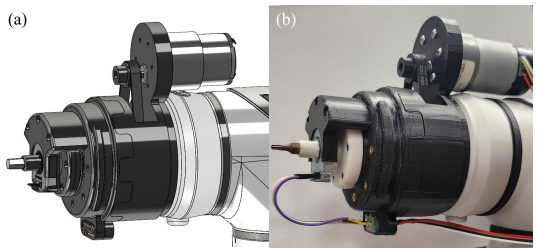

FIGURE 1. Proposed magnetic gear-based tool-changing module.

TABLE 1. Commercially available tool changer.

Model	Coupling Method	Actuation
Schunk SWS 005 [8]	taper and ball	pneumatic
ATI QC-11 [9]	taper and ball	pneumatic
GIMATIC EQC5 [10]	ball	electric motor
NORDBO NTC-E10 [11]	magnetic coupling	*EPM
TripleA Robotics WM1-K-04 [12]	kinematic coupling	passive

*EPM = electro-permanent magnet;

and unlocking the tool end-effectors. In this work, we have introduced the magnetic gear in the tool-changing mechanism to tackle the issues simply.

The magnetic gear is a remote power transmission using the magnetic force of permanent magnets (PMs). It was first proposed in 1980-1990 [13], [14] as the counterpart of mechanical gear. This unique non-contact transmission feature provides various advantages, such as high-backdrivability, transparency, and impact resistance. The magnetic coupling between input and output shows a spring-like characteristic, which enables sensorless torque control similar to the series elastic actuator [15]. Despite these attractive features, it had very limited application due to its low torque capability since only a small portion of PMs were engaged in magnetic coupling. After Atallah introduced the concept of coaxial magnetic gears (CMGs) [16], [17], which significantly enhance the torque density, introducing the use of the coaxial structure and a pole-piece ring (i.e., modulation ring) that makes all PMs engaging in the magnetic coupling, numerous research groups have conducted in-depth investigations into their practical applications, including wind turbine generator [18], electric vehicle [19], [20], marine applications [21], [22], robotic applications [15], [23], [24].

In this paper, we propose a novel coaxial magnetic gear-based tool-changing mechanism for a manipulator, and its feasibility is evaluated with bolting task as shown in Fig. 1. Thanks to the unique non-contact power transmission feature of the magnetic coupling, the proposed mechanism effectively interchanges the tools for specific tasks, solely relying on the magnetic force without additional actuation and intervention. In addition, the sensorless torque control capability of the magnetic gear enables the torque control of the tool without a torque sensor, which allows the manipulator to conduct various force/torque-based tasks.

The contributions of this work are as follows:

- This work is the first proposal of a tool-changing mechanism using a CMG.
- A simplified coupling mechanism of tool-changing mechanisms based on a CMG
- A sensorless torque control of a tool-changer
- A design and experimental validation of a CMG-based tool-changer

This paper is organized as follows with supplementary videos (Videos S1-S2), Section II describes the novel mechanical design of the coaxial magnetic gear-based tool-changing module and docking station for replacement. Based on our previous research regarding sensorless torque control strategy using characteristics of magnetic coupling [15], integrated control architecture was formulated in Section. III. Section IV represents the validation of the proposed tool-changing mechanism through experiments. The discussion and conclusion are followed in Section V and VI.

II. MECHANISM DESIGN

This section describes the concept and mechanical design of the proposed CMG-based tool-changing mechanism, mainly focusing on how the tool-changing module can be detached and attached.

A. COAXIAL MAGNETIC GEARS

The CMG consists of three main components: an inner rotor, an outer rotor, and a pole-piece ring, also known as the modulation ring (see Fig. 2(a)). Each of these rotors and the ring is constructed with a specific number of pole-pairs and ferromagnetic pieces. This particular arrangement generates magnetic coupling between each component with a specific transmission ratio. This transmission ratio, G, is determined by the following [23]:

$$N = p_i + p_o \tag{1}$$

$$G = \begin{cases} w_o/w_N = N/p_o & \text{when inner rotor fixed} \\ w_i/w_N = N/p_i & \text{when outer rotor fixed} \\ w_i/w_o = -p_o/p_i & \text{when pole-piece ring fixed} \end{cases} \tag{2}$$

where p_i, p_o, and N are the number of pole-pairs of the inner and outer rotor and ferromagnetic pieces of the modulation ring, respectively. w represents the angular velocity of corresponding parts (i.e., w_i: inner rotor, w_o: outer rotor; w_N: pole-piece ring).

In this work, we set the inner rotor as the input and the pole-piece ring as the output in order to maximize the transmission ratio (i.e., $G = N/p_i$) and the corresponding output torque. Each number of pole-pair and ferromagnetic pieces was selected based on the ripple factor to minimize the effects of ripple torque [25]. Additionally, we have used rectangle-shaped PMs, rather than customized arc-shape PMs, to reduce the cost of PMs. For the configuration of the magnets constituting the CMG, we introduced the Halbach array, one of the magnetic field concentration methods, to enhance torque density within the system, as shown in Fig. 2(b) [26]. Fig. 2(c)-(d) show the magnetic flux line

TABLE 2. Parameters of the tool-changing module.

Symbol	Parameter	Value	Unit
p_i	pole-pair of inner rotor	2	-
p_o	pole-pair of outer rotor	13	-
N	number of pole-pieces	15	-
G	transmission ratio	7.5	-
J_m	inertia of motor side	5.87e-3	$kg \cdot m^2$
B_m	damping of motor side	0.014	$Nm \cdot s/rad$
K_f	linearized magnetic spring stiffness	1.7314	Nm/rad
-	weight of tool-changing module	0.728	kg
-	weight of motor	0.2	kg
-	nominal power of motor	3	W
-	nominal torque of motor (w/ gearbox)	0.3	Nm
-	maximum transmittable torque of magnetic gear	2.42	Nm

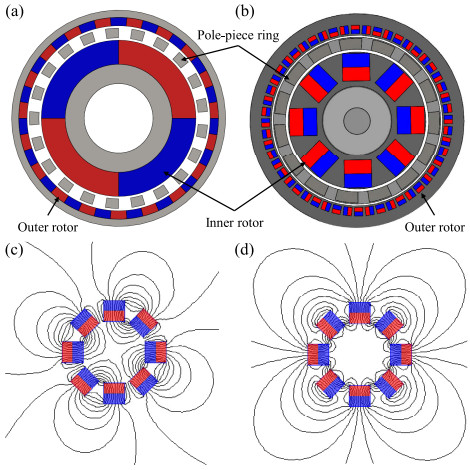

FIGURE 2. Schematics of CMGs (a) conventional CMGs, (b) Halbach array CMGs with rectangle-shape PMs. (c)-(d) Magnetic flux line comparison of the conventional array and Halbach array of the inner rotor with rectangle-shape PMs.

generated by the inner rotor magnet array with the same number of pole-pair but a different configuration using finite element method magnetics (FEMM) simulation [27]: the conventional arrangement in Fig. 2(c) and Halbach array configuration in Fig. 2(d). These illustrations demonstrate that the Halbach array effectively concentrates the magnetic flux radially in an outward direction, consequently increasing the torque capability of the magnetic gear. Interestingly, all the components (i.e., the rotors and ring in Fig. 2(b)) of the manufactured coaxial magnetic gear are mechanically isolated without any contact. Thus, each component can be easily disassembled from the others, but when assembled together, they can transmit torque due to the remote power transmission capabilities of the magnets. Additionally, because the magnetic gear teeth, formed through magnetic field harmonics, can deform under external loads unlike mechanical gears, they offer a virtual spring-like feature. Further details on this characteristic will be discussed in Section III. This unique property has been harnessed in the development of an automatic tool-changing mechanism in this study. The detailed parameters are summarized in Table 2.

B. TOOL-CHANGING MODULE

Fig. 3 shows the schematic of the proposed magnetic gear-based tool-changing mechanism, and it comprises two

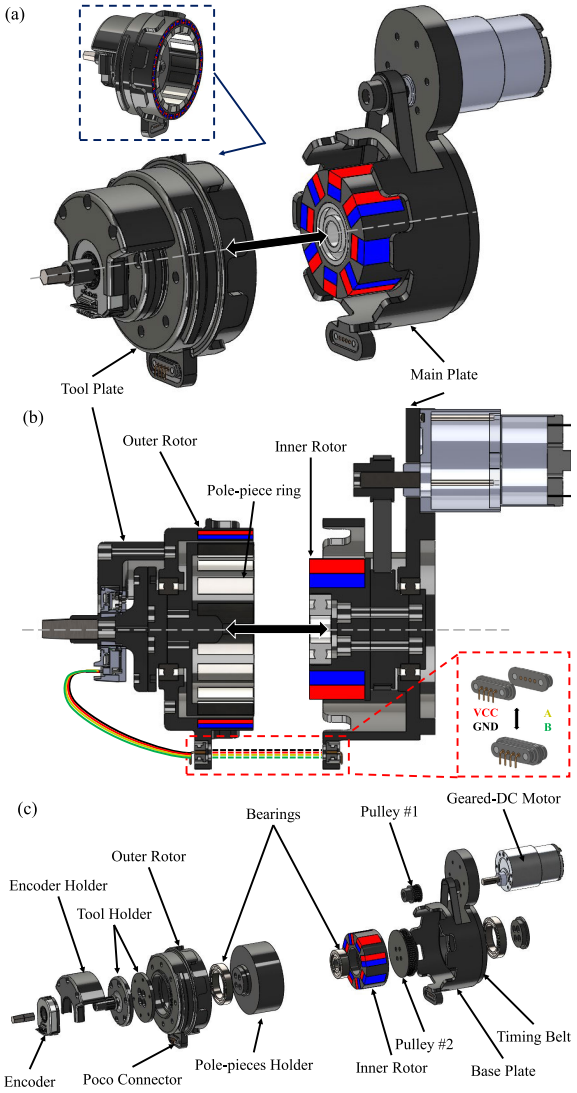

FIGURE 3. Schematics of the tool-changing module. (a) tool-changing module, (b) cross-section view, and (c) exploded view.

parts: the main plate and the tool plate. Since the unique feature of the magnetic coupling allows the non-contact power transmission, the two plates can be assembled and disassembled without any complex mechanical component but only utilize remote magnetic force for tool changing. To implement the proposed tool-changing mechanism, the following design has been introduced.

The main plate, which is intended to be attached to the end tip of the robotic manipulator, consists of three primary components (see Fig. 3(c)): the base plate, the inner rotor of the magnetic gear, and the geared-DC motor (JGB37-3530GB, Aslong). The inner rotor, consisting of multiple magnet pairs, is mounted on the base plate via a bearing, enabling free rotational motion relative to the base plate. In this configuration, a rotational motion of the inner rotor is connected to the geared-DC motor through two pulleys (pulley #1 and #2 in Fig. 3(c)) and a timing belt. Consequently, the geared-DC motor can control the rotational angle of the inner rotor.

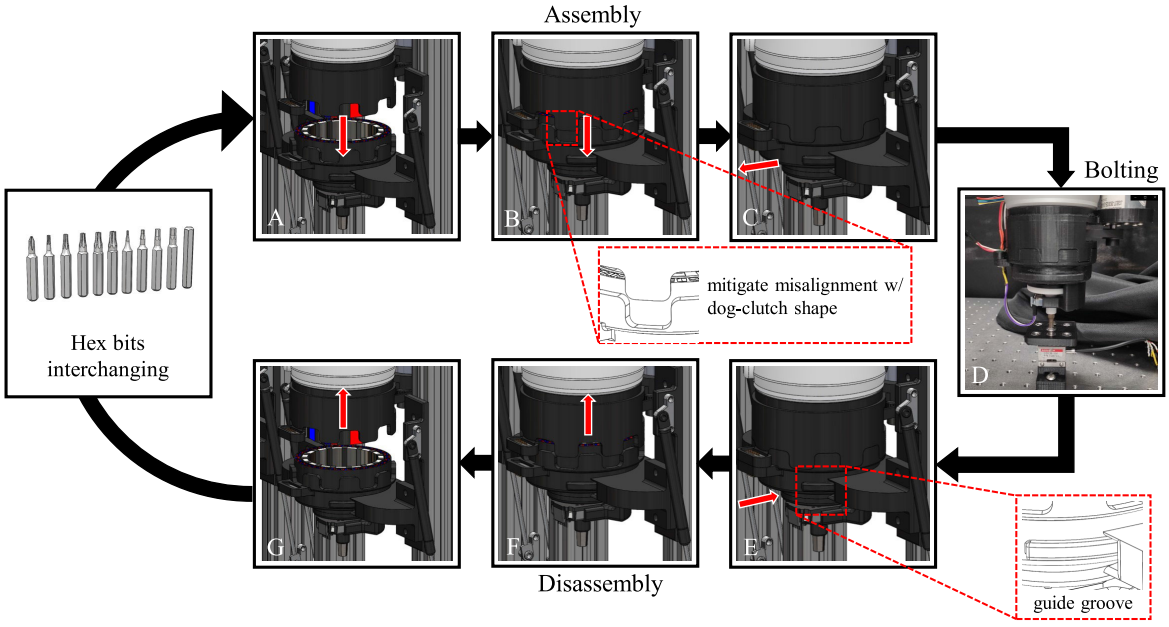

FIGURE 4. Overall assembly, tool operation, and disassembly procedures of proposed system.

The tool plate comprises the pole-pieces holder, outer rotor, encoder (AMT-103V, CUI), and tool. Multiple ferromagnetic pole-pieces are integrated into the pole-pieces holder to serve the function of the pole-piece ring, as shown in Fig. 2. The outer rotor incorporates several magnet pairs and is linked to the pole-pieces holder via a bearing, enabling free rotational movement relative to each other. The tool holder, which houses a tool, is connected to the pole-pieces holder, coupling their rotational motion, which is measured by the encoder. The electric power and signal from the encoder are transmitted to a controller through a pogo connector, which allows for the connection of the signal lines (see Fig. 3(b)), enabling the system to monitor the rotational angle of the tool and the pole-pieces holder.

Finally, the proposed design allows the two plates to be docked and merged into a unified form, configuring the coaxial magnetic gear structure, as illustrated in Fig. 2(b), thereby enabling torque transmission. The detailed assembly procedure is depicted in Fig. 4. To ensure that there is no relative rotational movement between the two plates for effective power transmission through magnetic coupling, we have introduced a dog-clutch mechanism on each side of the plates. When the two plates are brought together and engaged, the dog-clutches lock their relative rotational motion and correct any misalignment, guaranteeing an optimal assembled configuration.

The geared DC motor serves as an input source, and its rotational motion of the motor is ultimately transmitted to the tool through magnetic coupling. It is important to note that the motor was exclusively employed as an illustrative example for providing rotary motion to the magnetic gear, and as such, it can be substituted with any other type of actuator, such as a pneumatic rotary actuator or a joint of the manipulator, depending on specific applications. Furthermore, it is worth noting that the motor control is not involved or engaged in the tool-changing process, and there is no need for auxiliary actuation to facilitate the tool-changing.

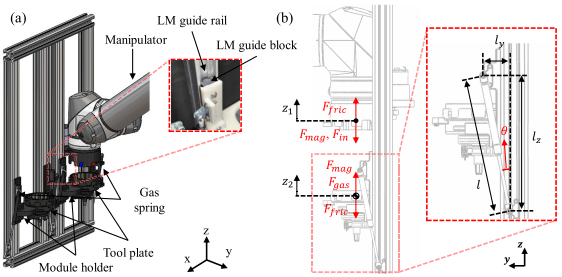

FIGURE 5. Schematics of the docking station (a) and its free body diagram (b).

In this work, the hex screwdriver bit was placed into the tool holder and was utilized to fasten a bolt, severing as a feasibility test.

C. DOCKING STATION

To address the concern of incomplete engagement if the tool plate remains stationary during the docking process, with potential risks to both the tool and the hardware, we have introduced an automated and robust docking procedure. This is achieved through the use of a docking station, depicted in Fig. 5(a). The docking station consists of a module holder, linear guide, and gas spring, providing a degree of freedom along the z-axis with added stiffness. In addition, the docking station allows for the tool plate to be smoothly slid and securely placed into the module holder along the guide groove, as illustrated in Fig. 4(E). The linear guide and the gas spring work in tandem to restrict the movement of the module holder along the z-axis.

Fig. 5(b) presents a simplified free-body diagram depicting the tool plate on the docking station and the main plate

on the manipulator during the tool docking process. In this diagram, F_{mag} represents the magnetic force between the main plate and the tool plate, while F_{fric} denotes the friction arising from the contact of the dog-clutch shape when there is misalignment. F_{in} signifies the input force (i.e., assembly downforce) originating from the manipulator, and F_{gas} represents the force generated by the gas spring. Note that F_{gas} is applied when z_2 falls below zero.

$$F_{assembly} = F_{mag} + F_{gas} - F_{fric} \tag{3}$$

$$F_{gas} = \begin{cases} 0 & z_2 \geq 0 \\ k\delta l cos(\theta) & z_2 < 0 \end{cases} \tag{4}$$

$$\delta l = l - \sqrt{l_y^2 + (l_z + z_2)^2} \tag{5}$$

$$\theta = atan(\frac{l_y}{l_z + z_2}) \tag{6}$$

Equation (3)-(6) represents the resultant force acting on the tool plate during the docking process along the z-axis. When viewed from an assembly standpoint, F_{mag} and F_{gas} contribute positively to the assembly force, while F_{fric} introduces a disruptive force that could potentially undermine the precision of the assembly. Here, k, δl, and l symbolize the stiffness, compressed distance, and equilibrium length of the gas spring (see Fig. 5(b)). It is worth noting that we have omitted the damping effect of the gas spring as the process is assumed to be quasi-static. As F_{gas} generates a positive assembly force that is linearly dependent on the downward offset (i.e., $-z$), it serves as a buffer to counteract the impact of F_{fric}. In the end, the inclusion of the gas spring ensures a secure engagement between the main and tool plates without causing damage to the hardware. The stiffness of the gas spring was carefully chosen to visibly demonstrate the gas spring effect of the docking station and to effectively compensate for misalignment, as established through experimental observations.

III. CONTROL ALGORITHM

A. TORQUE CONTROL OF TOOL-CHANGING MODULE

As stated in section II-A, the magnetic coupling has spring-like characteristics, and this spring-like feature can be utilized in sensorless torque control [15]. The torque of magnetic coupling is derived as follows [28]:

$$\tau = \tau_g \sin(\theta_e) \tag{7}$$

$$\theta_e = p_i\theta_m - N\theta_l \tag{8}$$

where θ_m and θ_l represent the rotational angles on the inner rotor (i.e., motor) and the pole-piece ring (i.e., load sides), respectively, while τ_g denotes the amplitude of the sine wave torque. θ_e is the electrical deflection angle of magnetic coupling. Fig. 6(a) illustrates the output torque of magnetic gear depending on the electrical deflection angle, θ_e, using FEMM [27].

Since the magnetic coupling shows the sinusoidal wave torque profile (see Fig. 6(a)), the stiffness of magnetic coupling could be approximately linearized within a confined operating region. Therefore, (7) represented as follows:

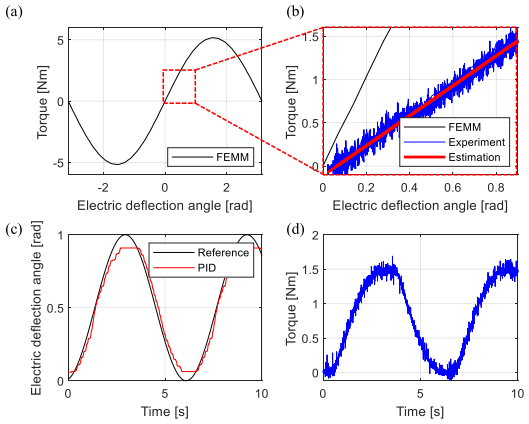

FIGURE 6. Simulated result of torque of magnetic gear (a). Experimental result of estimated stiffness of magnetic spring using PID controller: (b) estimated stiffness, (c) electrical deflection angle, and (d) torque.

$$\tau = K_f\theta_e \tag{9}$$

This assumption enables the linearization of the magnetic gear's dynamics and the application of linear control methodologies. More detailed information on the torque control of the magnetic gear can be found in our previous research [15].

To experimentally determine the stiffness of magnetic coupling, a proportional-integral-derivative (PID) controller was employed to control θ_e (see Fig. 6(c)) while a load cell (BDCM-100, BONGSHIN) measured the corresponding output torque (see Fig. 6(d)). Fig. 6(b) presents the experimentally estimated stiffness of the magnetic coupling, with a value of K_f at 1.7314 Nm/rad. This stiffness value determined here is employed for the sensorless torque control of the tool. Note that there was a discrepancy observed between the simulated and experimental outcomes. This will be thoroughly addressed in the discussion section. Furthermore, the maximum torque capacity (i.e., maximum transmittable torque) of the designed magnetic gear was measured to be 2.42 Nm. It is important to note that if the torque applied to the magnetic coupling exceeds this maximum capacity, a pole slip occurs, resulting in disengagement of the magnetic coupling, as discussed in our previous work [15]. This feature ensures hardware safety by preventing mechanical damage. The detailed specification of the tool-changing module is summarized in Table 2.

B. INTEGRATED CONTROL ALGORITHM WITH MANIPULATOR

In this work, a bolt-tightening demonstration was conducted to verify the feasibility of the proposed tool-changing module. To effectively utilize the tool-changing module for the task, it was imperative to have not just a robust torque controller but also an additional z-direction controller for the manipulator that can maintain a stable connection with the screw plate since the bolt will descend as it rotates.

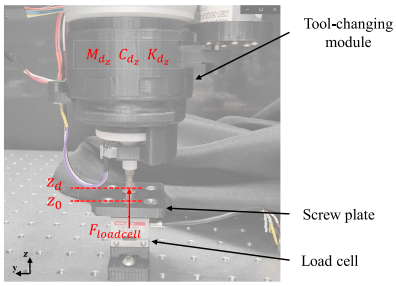

FIGURE 7. Schematic outline of bolting task.

Therefore, we have introduced an admittance controller for the manipulator along the z-direction in the operational space. Due to the absence of a torque/force sensor in each joint of the manipulator (RB-850, Rainbow Robotics), an additional load cell was temporarily implemented underneath the screw plate for the z-directional force feedback (see Fig. 7). To enable the robotic manipulator to mimic the behavior of having a virtual mechanical impedance, the admittance control law is calculated as follows [29]:

$$M_{d_z}(\ddot{z}_d - \ddot{z}_0) + C_{d_z}(\dot{z}_d - \dot{z}_0) + K_{d_z}(z_d - z_0) = F_{ext} \quad (10)$$

where M_{d_z}, C_{d_z}, and K_{d_z} are the z-directional desired mechanical impedance in the operational-space of the manipulator. z_0 is the z-directional equilibrium position of the admittance controller, and z_d is the z-directional desired reference of the manipulator. F_{ext} is external forces applied to the system. Eq. (10) implies that the virtual dynamics between the tool-changing module and screw plate are realized with respect to the equilibrium point by regulating the reference position of the manipulator. To secure contact between the hex screw bit of the tool-changing module and the screw plate, the equilibrium point, z_0, should be positioned beneath the contact point. We have updated the equilibrium point as the rotation of the load side of the magnetic gear (i.e., rotation of the hex screw bit) as follows:

$$z_0 = -p\theta_l - \alpha + z_{init} \quad (11)$$

$$\alpha = \int \delta dt, \quad (0 \le \alpha \le \alpha_{max}) \quad (12)$$

where p is the pitch of the screw, z_{init} is the initial value of the equilibrium, and α is the additional reference as a function of time. The δ and α_{max} are the tuning parameters that determine the rate change of the additional reference of the equilibrium point and its limit value. This control law gradually increases the equilibrium point until the interaction force reaches the threshold value, which is determined by the impedance value of the admittance controller. The integrated controller is shown in Fig. 8.

IV. EXPERIMENTS

The proposed magnetic gear-based tool-changing module was validated through two experiments: 1) tool replacement and 2) fastening the bolt under constant torque. Fig. 9(a)-(b) shows the experiment setup and its workflow. Fig. 9(a) A-D depicts the tool replacing experiment and Fig. 9(b) E-H shows the process of fastening the bolt (see supplementary Videos S1-S2). The experiments involved the use of a motor driver (Escon Module 24/2, Maxon) to control the geared-DC motor, and a microprocessor (LAUNCHXL-F28379D, Texas Instruments) was utilized to execute the torque controller for the magnetic gear. The high-level controller ran on Simulink Desktop Real-Time (Matlab R2022b, Mathworks), and communication between the high-level controller and the robotic manipulator was established using a TCP/IP interface.

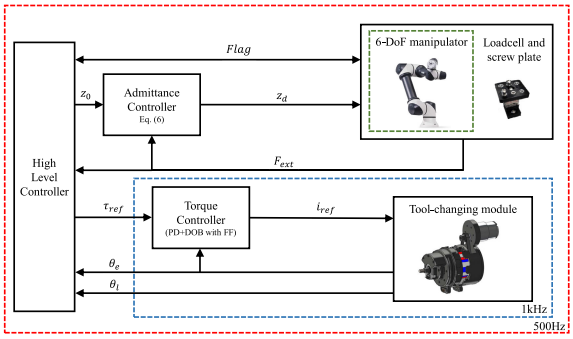

FIGURE 8. The control scheme of the magnetic gear-based tool-changing module.

A. TOOL-CHANGING

Fig. 9(a) A-D illustrates the procedure for swapping the tool plate using the magnetic coupling without the need for additional actuation. The docking station is instrumental in providing a reliable method for attaching and detaching the tool plate. It achieves this through the gas spring and an additional degree of freedom along the z-axis. As the tool plate is assembled, it exerts a positive force by moving z_2 (as seen in (3)) in the negative z-direction. This movement compensates for the frictional force (F_{fric}), ensuring a secure attachment. Fine-tuning the additional z_2 movement was necessary due to the nonlinearity of the magnetic coupling force (F_{mag}) and the frictional force (F_{fric}). In the case of detachment, the force of the gas spring becomes inactive once it has reached its maximum allowable stroke, holding the tool plate in a fixed position. The demonstration video shows the assembly and disassembly procedure with the docking station (see Video S1).

B. TIGHTENING THE BOLT

Fig. 9(b) E-H depicts the bolt-tightening process using the magnetic gear-based tool changer. Once the high-level controller received the signal indicating that the robotic manipulator had reached the predetermined bolt position, a torque command was generated for the torque controller. Concurrently, the admittance controller was engaged until the electric deflection angle, θ_e, of the magnetic gear (i.e., estimated torque) reached the corresponding reference electric deflection angle, θ_{e_ref} (i.e., target torque), with the equilibrium point of the admittance controller continuously updated to account for the load-side rotation. The experiment

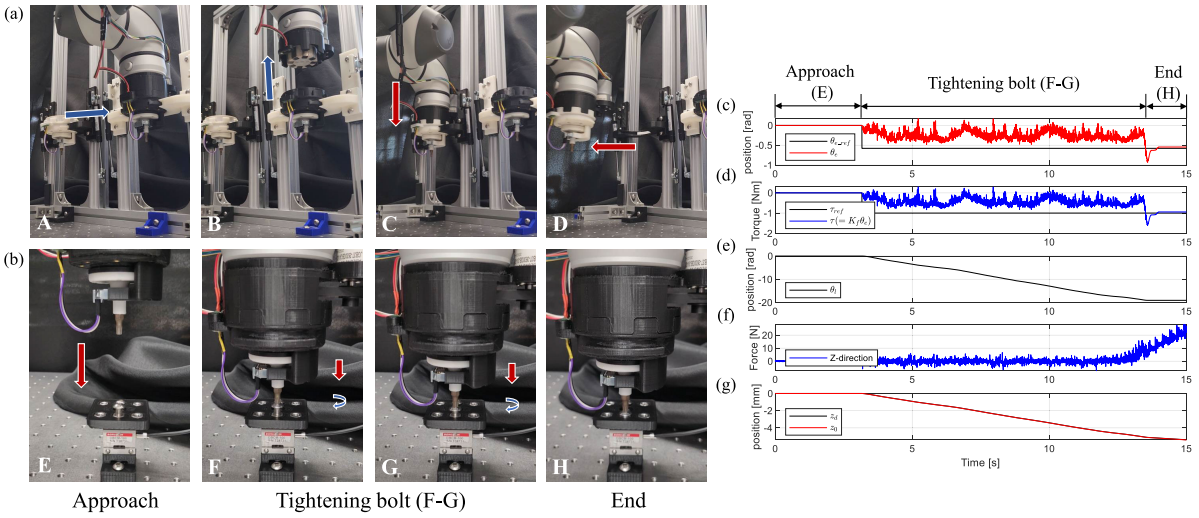

FIGURE 9. The experiment progress and results. (a) tool-changing sequence: (A-B) Detaching the tool plate; (C-D) Changing to another tool plate with a different screwdriver bit. (b) bolt-tightening process (E) Approaching the bolt; (F-G) Tightening the bolt using z-axis admittance controller to maintain continuous contact between the bolt and the bit (H) Completion of the task. (c)-(d) reference tracking of the electrical deflection angle and torque, and corresponding (e) load angle, (f) force, and (g) reference and equilibrium point of admittance controller.

result is shown in Fig. 9(c)-(g). As shown in Fig. 9(c)-(d), the torque controller effectively reaches the desired reference of the electrical deflection angle, which results in torque due to magnetic coupling. Fig. 9(c) represents the reference electrical deflection angle, θ_{e_ref}, and the electrical deflection angle, θ_e, and Fig. 9(d) illustrates the corresponding torque output. Note that the torque represented in Fig. 9(d) was calculated from the relation between the electrical deflection angle and the torque. Fig. 9(f)-(g) shows the forces from the load cell (see Fig. 7) and the equilibrium position of the admittance controller during bolting. The admittance controller shows a gradually increasing equilibrium position, meaning that the end of the tool maintains contact with the screw plate. The demonstration video illustrates the accomplishment of the bolting process using the suggested CMG-based tool-changing module and integrated controller (see Video S2).

V. DISCUSSION

We introduced a coaxial magnetic gear-based tool-changing mechanism that employs magnetic coupling for both tool replacement and torque control simultaneously. This non-contact power transmission mechanism offers several advantages, including high transparency, backdrivability, and hardware safety. In terms of design, the magnetic gear in the proposed system capitalizes on its inherent non-contact transmission capability to enhance hardware safety. This distinctive attribute of the magnetic gear plays a crucial role in isolating the powertrain, thereby ensuring the hardware's safety and functioning as an effective torque limiter. Although the implementation of an admittance controller, integrated with a 6-DoF T/F sensor, could potentially address this challenge, the physical isolation offered by the magnetic gear ensures that the integrity of the system is maintained independently of the performance of the controller.

However, there are several challenges that need to be addressed. Since the tool plate is connected to the main plate solely through magnetic force, the payload capacity of the tool plate is limited by magnetic coupling, consequently restricting its potential applications. Additionally, the output torque displayed considerable variances between the simulated and experimental findings (see Fig. 6(b)). This disparity is attributable to multiple factors: Firstly, it originates from the end-effects. Typically, 2D FEMM tends to overestimate performance as it fails to account for magnetic leakage and fringing, which are integral aspects of the end-effects. Secondly, the discrepancy may also be due to frictional losses arising from the hardware assembly and issues related to tolerance.

During the experiments, the success of the bolt-tightening task was determined by monitoring the electrical deflection angle of the magnetic gear. This angle serves as an indicator of the applied torque in a sensorless manner, which has the potential to decrease costs and increase the system's robustness. However, for tasks that require greater precision and accuracy, employing additional sensors could be considered to detect specific events during the operation.

We believe that this mechanism is well-suited for lightweight applications and scenarios where direct torque feedback is essential for precision control and protection of the system, such as tasks including assembling, impacting, and collaborating with humans. It is worth noting that despite the high transmission efficiency of magnetic gears, our prototype experiences some frictional losses due to the tolerances in the 3D-printed components. These challenges can be mitigated through hardware improvement in future work.

VI. CONCLUSION

In this paper, we proposed a coaxial magnetic gear-based tool-changing mechanism and docking station for

tool replacement. This system utilizes the CMGs for sensorless torque control, has resilience to external impacts due to non-contact power transmission, and offers tool interchangeability. Through experimental validation, we have demonstrated the feasibility and effectiveness of the proposed CMG-based tool-changing mechanism. We presented a control algorithm designed for bolting tasks, which combines a torque controller and an admittance controller to maintain a connection with the screw plate and the bolt. Despite some limitations, such as payload capacity constraints and frictional losses, this mechanism shows great promise for lightweight applications and tasks that demand direct torque feedback in rotational motion.

REFERENCES

[1] D. Mourtzis, *Design and Operation of Production Networks for Mass Personalization in the Era of Cloud Technology*. Amsterdam, The Netherlands: Elsevier, 2021.
[2] B. Dynamics. *Hey Buddy, Can You Give Me a Hand?*. Accessed: Sep. 30, 2023. [Online]. Available: https://www.youtube.com/watch?v=fUyU3lKzoio
[3] C. D. Bellicoso, K. Krämer, M. Stäuble, D. Sako, F. Jenelten, M. Bjelonic, and M. Hutter, "ALMA–articulated locomotion and manipulation for a torque-controllable robot," in *Proc. Int. Conf. Robot. Autom. (ICRA)*, May 2019, pp. 8477–8483.
[4] OnRobot. *Dual Quick Changer*. Accessed: Sep. 30, 2023. [Online]. Available: https://onrobot.com/en/products/dual-quick-changer
[5] I. A. Anderson, T. A. Gisby, T. G. McKay, B. M. O'Brien, and E. P. Calius, "Multi-functional dielectric elastomer artificial muscles for soft and smart machines," *J. Appl. Phys.*, vol. 112, no. 4, Aug. 2012.
[6] M. Behl, K. Kratz, J. Zotzmann, U. Nöchel, and A. Lendlein, "Reversible bidirectional shape-memory polymers," *Adv. Mater.*, vol. 25, no. 32, pp. 4466–4469, 2013.
[7] Festo. *The Multichoicegripper*. Accessed: Sep. 30, 2023. [Online]. Available: https://www.festo.com/group/en/cms/10221.htm
[8] Schunk. *Sws 005*. Accessed: Sep. 30, 2023. [Online]. Available: https://schunk.com/gb/en/automation-technology/change-systems/sws/c/PGR_1135
[9] ATI. *Qc-11*. Accessed: Sep. 30, 2023. [Online]. Available: https://www.ati-ia.com/products/toolchanger/QC.aspx?ID=QC-11
[10] Gimatic. *Eqc05*. Accessed: Sep. 30, 2023. [Online]. Available: https://shop.gimatic.com/en/eqc
[11] Nordbo Robotics. *Nordbo Ntc-e10*. Accessed: Sep. 30, 2023. [Online]. Available: https://www.nordbo-robotics.com/components/tool-changer.
[12] TripleA Robotics. *Wm1-k-04*. Accessed: Sep. 30, 2023. [Online]. Available: http://triplea-robotics.com/tool-changer/.
[13] D. E. Hesmondhalgh and D. Tipping, "A multielement magnetic gear," *IEE Proc. B Electric Power Appl.*, vol. 127, no. 3, p. 129, 1980.
[14] K. Tsurumoto and S. Kikuchi, "A new magnetic gear using permanent magnet," *IEEE Trans. Magn.*, vol. M-23, no. 5, pp. 3622–3624, Sep. 1987.
[15] H. Song, E. Lee, H.-T. Seo, and S. Jeong, "Magnetic gear-based actuator: A framework of design, optimization, and disturbance observer-based torque control," *IEEE Robot. Autom. Lett.*, vol. 8, no. 11, pp. 7050–7057, Nov. 2023.
[16] K. Atallah and D. Howe, "A novel high-performance magnetic gear," *IEEE Trans. Magn.*, vol. 37, no. 4, pp. 2844–2846, Jul. 2001.
[17] K. Atallah, S. D. Calverley, and D. Howe, "Design, analysis and realisation of a high-performance magnetic gear," *IEE Proc. Electric Power Appl.*, vol. 151, no. 2, p. 135, 2004.
[18] H. Polinder, J. A. Ferreira, B. B. Jensen, A. B. Abrahamsen, K. Atallah, and R. A. McMahon, "Trends in wind turbine generator systems," *IEEE J. Emerg. Sel. Topics Power Electron.*, vol. 1, no. 3, pp. 174–185, Sep. 2013.
[19] L. Jing, W. Tang, T. Wang, T. Ben, and R. Qu, "Performance analysis of magnetically geared permanent magnet brushless motor for hybrid electric vehicles," *IEEE Trans. Transport. Electrific.*, vol. 8, no. 2, pp. 2874–2883, Jun. 2022.
[20] C. Liu, J. Yu, and C. H. T. Lee, "A new electric magnetic-geared machine for electric unmanned aerial vehicles," *IEEE Trans. Magn.*, vol. 53, no. 11, pp. 1–6, Nov. 2017.
[21] G. Cooke, R.-S. Dragan, R. Barrett, D. J. Powell, S. Graham, and K. Atallah, "Magnetically geared propulsion motor for subsea remote operated vehicle," *IEEE Trans. Magn.*, vol. 58, no. 2, pp. 1–5, Feb. 2022.
[22] H. Baninajar, S. Modaresahmadi, H. Y. Wong, J. Bird, W. Williams, and B. Dechant, "Designing a Halbach rotor magnetic gear for a marine hydrokinetic generator," *IEEE Trans. Ind. Appl.*, vol. 58, no. 5, pp. 6069–6080, Sep. 2022.
[23] E. Lee, H. Song, J. Jeong, and S. Jeong, "Mechanical variable magnetic gear transmission: Concept and preliminary research," *IEEE Robot. Autom. Lett.*, vol. 7, no. 2, pp. 3357–3364, Apr. 2022.
[24] B. Praslicka, M. Johnson, E. Plugge, N. Palmer, D. F. Knight, A. White, T. Simms, D. Zamarron, and H. A. Toliyat, "Design and analysis of a novel, low-cost, high-speed cycloidal magnetic gear for aerospace servo actuator applications," *IEEE/ASME Trans. Mechatronics*, pp. 1–12, 2023.
[25] B. Praslicka, M. C. Gardner, M. Johnson, and H. A. Toliyat, "Review and analysis of coaxial magnetic gear pole pair count selection effects," *IEEE J. Emerg. Sel. Topics Power Electron.*, vol. 10, no. 2, pp. 1813–1822, Apr. 2022.
[26] L. Jian and K. T. Chau, "A coaxial magnetic gear with Halbach permanent-magnet arrays," *IEEE Trans. Energy Convers.*, vol. 25, no. 2, pp. 319–328, Jun. 2010.
[27] D. C. Meeker. (Apr. 21, 2019). *Finite Element Method Magnetics*. Version 4.2, Accessed: Jun. 23, 2023. [Online]. Available: https://www.femm.info
[28] R. Montague, C. Bingham, and K. Atallah, "Servo control of magnetic gears," *IEEE/ASME Trans. Mechatronics*, vol. 17, no. 2, pp. 269–278, Apr. 2012.
[29] C. Ott, R. Mukherjee, and Y. Nakamura, "Unified impedance and admittance control," in *Proc. IEEE Int. Conf. Robot. Autom.*, May 2010, pp. 554–561.

HANGYEOL SONG received the B.S. and M.S. degrees in mechanical engineering from Sogang University, Seoul, South Korea, in 2019 and 2023, respectively. He is currently a Research Assistant with the Department of Mechanical Engineering, Sogang University. His research interests include mechanisms design and control for small-to-medium-sized robotic systems.

JUNGWOO HUR is currently pursuing the B.S. degree in mechanical engineering with Sogang University, Seoul, South Korea. He is actively engaged as an Undergraduate Researcher with the Robotics and Intelligent Mechanisms Laboratory, Sogang University. His research interests include the design and control of dynamic interaction robots.

SEOKHWAN JEONG (Member, IEEE) received the B.S. degree in mechanical engineering from Yonsei University, Seoul, South Korea, in 2013, and the M.S. and Ph.D. degrees in mechanical engineering from Korea Advanced Institute of Science and Technology (KAIST), Daejeon, South Korea, in 2015 and 2018, respectively. From 2018 to 2020, he was a Postdoctoral Researcher with the RoboMed Laboratory, Department of Biomedical Engineering, Georgia Institute of Technology, Atlanta, GA, USA. He is currently an Assistant Professor with the Department of Mechanical Engineering, Sogang University, Seoul, and a Principal Investigator of the Robotics and Intelligent Mechanisms (RIM) Laboratory (https://rim.sogang.ac.kr/). His research interests include novel actuation mechanisms and designs, robotic hands, prosthetic hand systems, sensor designs, and control.